Stick-slip friction and nucleation dynamics of ultrathin liquid films

I. S. Aranson,[1] L. S. Tsimring,[2] and V. M. Vinokur[1]
[1]*Argonne National Laboratory, 9700 South Cass Avenue, Argonne, Illinois 60439*
[2]*Institute for Nonlinear Science, University of California, San Diego, La Jolla, California 92093-0402*
(Received 3 October 2001; published 14 February 2002)

We develop a theory for stick-slip motion in ultrathin liquid films confined between two moving atomically flat surfaces. Our model is based on the hydrodynamic equation for flow coupled to the dynamic order parameter field describing the ''shear melting and freezing'' of the confined fluid. This model successfully accounts for the observed phenomenology of friction in ultrathin films, including periodic and chaotic sequences of slips, transitions from stick-slip motion to steady sliding, and ultrasound generation.

DOI: 10.1103/PhysRevB.65.125402 PACS number(s): 62.20.Fe, 62.20.Qp, 68.60.−p

I. INTRODUCTION

The nature of sliding friction is a fundamental physical problem of prime practical importance.[1,2] While the possibility to create low-friction surfaces and lubricant fluids has been ubiquitous for almost all engineering applications, it has become crucial for the design of modern microminiature devices such as information storage and microelectromechanical systems, where low friction without stick-slip (or interrupted) motion is necessary.

Studies of friction between atomically flat mica surfaces separated by an ultrathin layer of lubricant have revealed a striking phenomenon:[3] in a certain range of experimental parameters the fluid exhibited solidlike properties, in particular, a critical yield stress leading to stick-slips similar to that in solid-on-solid dry friction processes[5] with the transition to sliding above critical velocity $V_c \sim 1$ μm/s. This behavior was attributed to the confinement-induced freezing of the lubricant and its recurring melting due to increased shear stress: as the fluid thickness is reduced to several molecular layers, it freezes, but when the shear stress exceeds some critical value, it melts. This behavior was confirmed by molecular dynamics (MD) simulations,[6,7] which indicated ordering of the fluid due to confinement by the walls.

A quest for the quantitative description of stick-slip lubricant dynamics motivated several theoretical works.[8–10] An important step has been made by Carlson and Batista[10] who proposed a phenomenological constitutive relation connecting the frictional forces to velocity and coordinates via the order-parameter-like state variable reflecting the degree of melting. This model successfully described some of the observed phenomenology of the experiment[3] and gave insight into the dynamics. Yet many important questions including the very mechanism of the onset of the stick-slip remain unresolved. In particular, MD simulations of Ref. 6 give the critical velocity $V_c \sim 10$ m/s which exceeds the experimental value by many orders. This apparent disagreement was attributed by Persson[9] to complex nucleation dynamics of stress domains and the importance of thermally activated processes in the shear melting transition.

In this paper we develop a theory of stick-slip motion in ultrathin liquids based on equations for the flow coupled to the equation for the order parameter (OP) for the melting transition in the presence of shear stress. We propose that the shear melting is controlled by the stress tensor rather than the sliding velocity as assumed in Ref. 10. Making use of the generalized Lindemann criterion, we combine shear and thermodynamic melting within a unified description. Using this approach we describe the onset of stick-slip motion as a function of the film thickness and temperature, and determine the dynamic phase diagram. We demonstrate that random nucleation of droplets of the fluid phase during the motion leads to an irregular temporal distribution of slip events and to ultrasound radiation. Admittedly, our approach is phenomenological in nature; it is not justified from first-principles calculations and cannot be used for a precise estimate of experimental parameters. Nevertheless, it captures all observed experimental phenomenology, results in a correct order of magnitude estimate of the critical velocity, and gives insights into the problem.

The structure of the article is the following. In Sec. II we describe the general formulation of our model. In Sec. III we introduce the thin-layer approximation. Using this approximation, we reduce the model to a relatively simple system of equations for averaged shear stress and deviation of the order parameter. In Sec. IV we study the stick-slip dynamics for spatially uniform motion. In that section we also compare our results for the critical velocity with the experimental values. In Sec. V we study the nucleation dynamics of liquid phase droplets in the overheated solid and connect it to irregularity in stick-slip sequences. Finally, in Sec. VI we investigate the generation of ultrasound by stick-slip events.

II. MODEL

The simplified setup of a friction experiment is shown in Fig. 1. The upper plate is sliding with the velocity V on a thin-layer of lubricant with thickness h. The ''free end'' of the spring, representing the overall elastic properties of the friction device, is pulled with constant velocity $\overline{V}$. The resulting friction force F is proportional to the deflection of the spring.

The flow of lubricant satisfies the momentum conservation law

$$\rho_0 \frac{Dv_i}{Dt} = \frac{\partial \sigma_{ij}}{\partial x_j}, \tag{1}$$

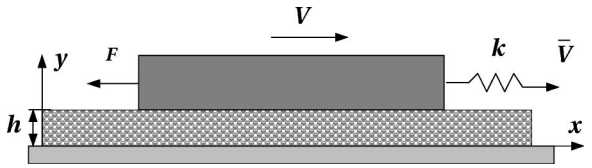

FIG. 1. Setup of typical friction experiment. The upper plate is sliding on a flat substrate covered by the lubricant with thickness h. A spring (spring constant k) is connected to the block and the "free end" of the spring moves with the constant pulling velocity $\bar{V}$.

where v_i is a component of the fluid velocity, $D/Dt=\partial_t+\mathbf{v}\nabla$ is the material derivative, and ρ_0 is the density of fluid. Assuming incompressibility we set $\rho_0=1$ and $\mathrm{div}\mathbf{v}=0$.

The stress tensor σ_{ij} is described by the Maxwell-type stress-stain relation, widely used in the boundary lubrication theory of friction:[1,2]

$$\partial_t\sigma_{ij}+\eta\sigma_{ij}=\mu S_{ij}, \tag{2}$$

where $S_{ij}=\partial v_i/\partial x_j+\partial v_j/\partial x_i$ is the strain rate tensor, μ is the shear modulus, and η is the shear stress relaxation rate. Thus, the stress-strain relation includes both viscous flow and elastic restoring forces. The microscopic mechanism of the stress relaxation can be attributed to nucleation and the motion of dislocations in the solidlike phase of the lubricant. The conventional shear viscosity is defined as $\nu=\mu/\eta$.

To describe the dynamic phase transition between solid and fluid states we take into account that the stress relaxation rate η is itself a function of the physical state of the material quantified near the melting transition by the OP ρ which is defined in such a way that $\rho=1$ corresponds to the solid state and $\rho=0$ to the liquid state. The physical interpretation of the OP for various systems can be different, but for crystalline solids ρ can be related to the dislocation density. We restrict ourselves to the simplest dependence of the stress relaxation rate on ρ: $\eta=\eta_0(1-\rho)$, $\eta_0=\mathrm{const}$. This choice assures that Eq. (2) gives Hook's law for the pure solid ($\rho=1$) and the viscous stress-strain relation for the Newtonian fluid with $\rho=0$. For the lubricant used in Ref. 3 the bulk value of η_0 at normal pressure is $O(10^{10})$ s^{-1}, and it decreases by several orders of magnitude at large pressures.[3,4]

In the spirit of the phenomenological theory of first-order phase transitions, we postulate that the OP for melting transition obeys the scalar Ginzburg-Landau equation

$$\partial_t\rho=-\frac{\delta\mathcal{F}}{\delta\rho}, \tag{3}$$

where the free energy $\mathcal{F}\sim\int d\mathbf{r}[D|\nabla\rho|^2+f(\rho)]$ includes the "local potential energy" $f(\rho)$ and the diffusive coupling $D|\nabla\rho|^2$ contributions. The diffusion constant D can be estimated as $l_0^2\tau_0^{-1}$, where τ_0 and l are the characteristic time and length, correspondingly; l is of the order of the lattice constant or intermolecular distance, $a\sim1$ nm, and time τ_0 is expressed through the sound velocity $c_s\sim10^3$ m/s, $\tau_0\approx l/c_s\sim10^{-12}$ s. The potential energy density $f(\rho)$ should have extrema at $\rho=0$ and $\rho=1$ corresponding to uniform solid and liquid phases. We approximate $f(\rho)$ by a quartic polynomial with three extrema at $\rho=0,1$ and $\rho=\delta$, so the order parameter equation becomes

$$\tau_0\partial_t\rho=l^2\nabla^2\rho-\rho(1-\rho)(\delta-\rho). \tag{4}$$

The control parameter δ is proportional to the temperature T. Since the melting of the lubricating layer occurs under out-of-equilibrium conditions, it is characterized by two critical temperatures T_1, corresponding to an instability of the overcooled liquid, and T_2, the stability limit of the overheated solid phase.[11,12] The thermodynamic melting temperature T_m is confined between these limits: $T_1<T_m<T_2$. The parameter δ is expressed in the form

$$\delta=(T-T_1)/(T_2-T_1). \tag{5}$$

Now we have to relate the solid instability temperature T_2 to the stress generated in the process of motion. According to the Lindemann hypothesis, at $T=T_2$ the mean-square displacement $\langle u^2\rangle=\tilde{c}_{\mathcal{L}}^2a^2$, where $\tilde{c}_{\mathcal{L}}^2$ is the numerical factor ("Lindemann number"). In the absence of shear deformations the temperature mean-square displacement $\langle u^2\rangle$ is related to the temperature as $\langle u^2\rangle=T/\mu a$. For averaged shear displacements the following relation holds: $\langle u^2\rangle=\sigma^2a^2/\mu^2$, where $\sigma\equiv\sigma_{xy}$ is the shear stress. Assuming independence of thermal fluctuations and shear, one can present the mean-square displacement field under shear stress in the form

$$\langle u^2\rangle\simeq\frac{T}{\mu a}+\frac{\sigma^2a^2}{\mu^2}, \tag{6}$$

where the first term on the right-hand side stands for the average thermal displacement, while the second term expresses the shear-induced displacement field. Equation (6) implies that the solid phase instability can stem not only from the thermal fluctuations, but also from the shear stresses. At zero physical temperature the instability can be caused by the shear only. This concept of *shear-induced melting* generalizes the hypothesis of the dynamic disorder-driven melting introduced in earlier work.[13] It finds support in the molecular dynamic simulations of the system under stress; see, e.g., Ref. 14. Although we apply the macroscopic concepts of free energy and shear to fairly thin system (under ten layers across), the continuum description can be supported by the fact that elasticity based estimates of the melting temperature (the temperature at which shear modulus vanishes) are in fairly good agreement with empirical data. Since melting is an inherently short-wave phenomenon, this offers some empirical support to the possibility of using the concept of shear until almost the atomic scale. Thus, we expect that our analysis will reproduce qualitative features of the shear melting in thin films and possibly will result in correct order of magnitude estimates for critical velocity and other observed quantities.

Since at $T=T_2$ the relation $\langle u^2\rangle=\tilde{c}_L^2a^2$ holds, at $T=T_2$, Eq. (6) yields

$$T_2=T_2^0-\sigma^2a^3/\mu, \tag{7}$$

where $T_2^0 = c_L^2 \mu a^3$. Substituting Eq. (7) into the expression for the control parameter δ, Eq. (5), one derives in the first order

$$\delta = \delta_0 + \sigma^2/\sigma_0^2, \tag{8}$$

where $\delta_0 = (T - T_1)/(T_2^0 - T_1)$ and $\sigma_0^2 = \mu(T_2^0 - T_1)/\delta_0 a^3$ is the yield shear stress.

III. THIN-LAYER APPROXIMATION

In the thin-layer approximation, the thickness of the lubricant layer h is small so that the dependence of the shear stress σ and other stress components on the transverse coordinate y is neglected in the leading order. Now we can further simplify the OP dynamics. Since the walls favor the formation of a solid, the boundary conditions for the OP are $\rho(0) = \rho(h) = 1$, and the bulk variations of the OP are small as compared to 1. Let us seek the solution in the form

$$\rho(x,y,t) = 1 - A(x,t)\sin\left(\frac{\pi y}{h}\right), \tag{9}$$

where $A \ll 1$ is the slowly varying amplitude. Substituting Eq. (9) into Eq. (4) and making use of the standard orthogonalization procedure leads to

$$\partial_t A = \partial_x^2 A + \left(\delta - 1 - \frac{\pi^2}{h^2}\right)A + \frac{16 - 8\delta}{3\pi}A^2 - \frac{3}{4}A^3, \tag{10}$$

where $\delta = \delta_0 + \sigma^2$, and the variables are rescaled as $x/l \to x, t/\tau_0 \to t, \sigma_{xy}/\sigma_0 \to \sigma, V \to V/(l/\tau_0)$, and $\eta_* \to \eta_0 \tau_0$.

After integrating over the width of the sample, Eq. (2) yields in the leading order

$$\partial_t \sigma + \frac{2\eta_*}{\pi} A\sigma = \frac{\mu V}{h\sigma_0} + \frac{\mu}{\sigma_0}\partial_x U, \tag{11}$$

where

$$U = \frac{1}{h}\int_0^h v_y dy \tag{12}$$

is the y component of the flow velocity averaged over the width of the sample. Here we used nonslip condition for the x component of the fluid velocity, which yields $v_x(h) - v_x(0) = V = \text{const}$, where V is the relative velocity of the upper plate with respect to the bottom.

Now, integrating Eq. (1) for the y component of the velocity one obtains

$$\partial_t U = \frac{\sigma_0 \tau_0^2}{l^2}\partial_x \sigma. \tag{13}$$

Here we assume that the hydrodynamic velocity is small and neglect terms $\mathbf{v}\nabla\mathbf{v}$. Thus, we obtain two coupled equations

$$\partial_t \sigma = -\frac{2\eta_*}{\pi} A\sigma + \frac{v_0}{h} + \nu S, \tag{14}$$

$$\partial_t S = \partial_x^2 \sigma - \zeta S, \tag{15}$$

where $v_0 = \mu V/\sigma_0$ is the rescaled velocity of the top plate, and $S = l^2/(\tau_0^2 \sigma_0)\partial_x U$, and $\nu = \mu/(l/\tau_0)^2 = O(1)$. The term ζS has been added to Eq. (15) in order to account for radiation losses of sound due to its leakage into the substrate. As one sees from Eqs. (14), and (15), for $A \to 0$ (solid phase) the above system is reduced to the wave equation $\partial_t^2 S = \nu \partial_x^2 S - \zeta \partial_t S$; i.e., it describes the propagation of shear elastic waves with sound velocity $c_s = \sqrt{\nu}$ and radiation decay rate ζ.

The pulling velocity $\overline{V}$ does not necessarily coincide with the upper plate velocity V; see Fig. 1. In a standard friction experiment, the upper plate is pulled via a spring with stiffness k. The relation between the position of the upper plate X, friction force F, and the position of the spring (neglecting masses of the spring and upper plate) reads $F = k(\overline{V}t - X)$. Since $F \sim \int_0^L \sigma(x)dx$ and $V = dX/dt$, the difference between the plate velocity V and pulling velocity $\overline{V}$ can be neglected for stiff enough springs.

IV. STICK-SLIP MOTION

First we discuss spatially uniform motion. In this case Eqs. (10), (14), and (15) are reduced to a pair of coupled ordinary differential equations (ODE's):

$$\partial_t A = \left(\delta - 1 - \frac{\pi^2}{h^2}\right)A + \frac{16 - 8\delta}{3\pi}A^2 - \frac{3}{4}A^3, \tag{16}$$

$$\partial_t \sigma = -\frac{2\eta_*}{\pi} A\sigma + \frac{v_0}{h}. \tag{17}$$

Above the melting temperature $\delta_0 > 1$, the solid phase of the lubricant is formed due to the proximity-to-the-walls effect. In the experimentally relevant limit $\eta_*, v_0 \ll 1$ Eqs. (16) and (17) can be investigated analytically using the bifurcation analysis and the multiscale technique with σ being a slow and A being a fast variable. Stick-slips are described by the limit cycle on the σ-A plane. The bifurcations among different regimes depend on the relative position of the nullclines which are defined by the conditions $d\sigma/dt = 0$ and $dA/dt = 0$. The slow-motion nullcline determined by Eq. (17) is of the form

$$\frac{2\eta_*}{\pi}\sigma A = v_0/h. \tag{18}$$

The manifold of fast motions consists of two separate curves

$$A = 0, \tag{19}$$

$$\left(\delta - 1 - \frac{\pi^2}{h^2}\right) + \frac{8}{3\pi}(2 - \delta)A - \frac{3}{4}A^2 = 0. \tag{20}$$

Fixed points of Eqs. (16) and (17), i.e., steady sliding regimes, correspond to the intersections of nullclines. The limit cycle can be approximated by two segments lying on two different nullclines of fast motion and two lines $\sigma = \text{const}$ which describe the rapid transitions from one branch of the

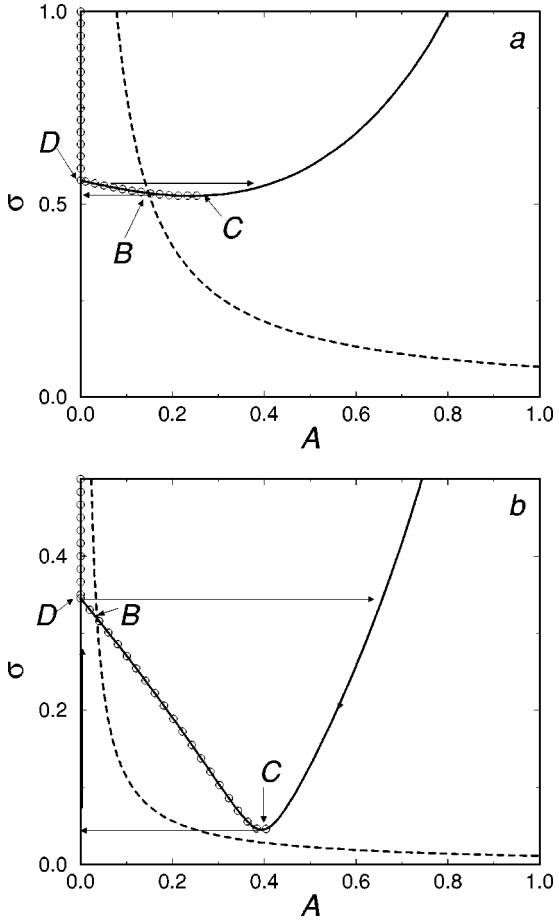

FIG. 2. Phase portraits of spatially uniform equations (10) and (14) in the regime of stick-slip motion for $\delta_0=1.3$. Solid lines show the nullclines of fast motion, Eqs. (19) and (20); dashed line indicates the nullcline of slow motion Eq. (18). The nullclines intersect in point *B*, and point *C* shows $d\sigma/dA=0$. Panel (a) ($h=4, v_0/\eta^*=0.2$) corresponds to the neighborhood of the continuous transition from stick-slip to sliding. The limit cycle vanishes smoothly when points *B* and *C* merge with an increase of v_0. Panel (b) ($h=4.85, v_0/\eta^*=0.03$) corresponds to the neighborhood of the discontinuous transition from stick-slip to sliding at larger *h*. The limit cycle disappears abruptly with hysteresis when point *C* touches the nullcline of slow motion Eq. (18) (dashed line), with an increase of v_0. The unstable branches of the nullclines are shown by lines with open circles.

nullcline, Eqs. (19) and (20), to another; see Fig. 2. The segment of fast-motion nullcline (20) left of point *C* is unstable. Therefore the trajectory slides down along fast-motion nullcline up to point *C* and then falls to the nullcline $A=0$. The nullcline (19) is unstable above point *D* given by the condition $\delta=1+\pi^2/h^2$. Thus, above this point the trajectory switches to nullcline (20).

It is easy to estimate the duration of stick (T_{stick}) and slip (T_{slip}) phases for $v_0\to 0$. Since the stick corresponds to motion along nullcline $A=0$, from Eq. (17) we obtain $T_{stick}\sim 1/v_0$. During the slip phase *A* and σ are related according to Eq. (20), and since for slip $A\sigma\sim O(1)\neq 0$ [see, e.g., Fig. 2(b)], from Eq. (17) one obtains $T_{slip}\sim 1/\eta_*$ if $\eta_*\gg v_0$. Thus, one obtains $T_{stick}\gg T_{slip}\gg 1$ for small η_*.

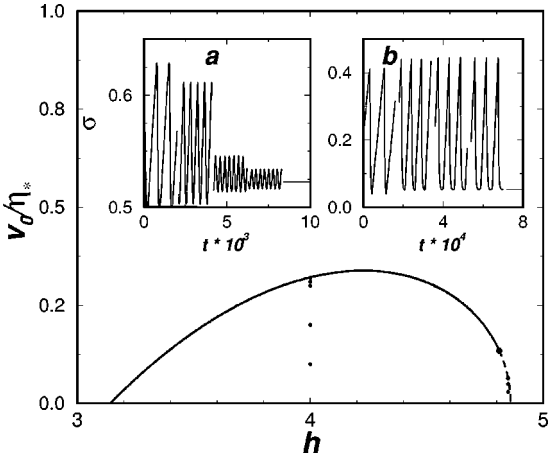

FIG. 3. Phase diagram of lubrication regimes at $\delta_0=1.3$. The solid line indicates the continuous transition from stick-slip to sliding, and the dashed line corresponds to the hysteretic abrupt transition. Insets a and b show normalized shear stress σ vs time for $\eta_*=0.01$ at two different values of *h* corresponding to continuous and discontinuous transitions, and several values of v_0/η_* approaching the transition line (dots in the main plot): $h=4$, $v_0/\eta_*=0.1$, 0.2, 0.3, 0.31, 0.32 (a) and $h=4.85$ $v_0/\eta_*=0.03$, 0.05, 0.064, 0.0645, 0.065 (b).

For $\eta_*\to 0$ the transition from stick-slips to continuous sliding corresponds to the intersection of the slow motion manifold with the minimum of the fast-motion manifold $\sigma=f(A)$, i.e., $d\sigma/dA=0$ shown in Fig. 2 by point *C*. The limit cycle vanishes smoothly if points *B* and *C* merge; see Fig. 2(a). It corresponds to a change of stability of the fixed point *B*. In this case one has supercritical Hopf bifurcation to limit the cycle with a decrease of v_0.

Another scenario occurs when there is more then one intersection point between fast and slow manifolds; see Fig. 2(b). One point *C* touches the slow manifold, the period of the limit cycle diverges, and the limit cycle disappears abruptly with hysteresis.

Figures 3 and 4 illustrate the transition from continuous sliding to the stick-slip motion. As one can see from Figs. 3 and 4, stick-slips are possible only in relatively thin-layers. In thick layers, sliding is steady since the lubricant in the bulk is always in a fluid state. The critical thickness h_c is determined by the stability condition $d\sigma/dA=0$ derived from Eq. (20): $h_c=\pi/\sqrt{\delta_0-1+64(2-\delta_0)^2/27\pi^2}$. We find that for *h* close to h_c transition from stick-slip to sliding is always abrupt and has a hysteretic character (see Fig. 4 and Fig. 3, inset b). For the chosen parameters, the ''friction law'' σ vs v_0 has a minimum (Fig. 4, inset, curve 2), as is common for a typical dry friction behavior.[1] For smaller δ_0 the transition is continuous (inset a in Fig. 3, curve 3 in Fig. 4, inset). For $h<h_0=\pi$ the dry friction without stick slip occurs because the viscous friction force becomes larger than the dry friction one, curve 1 in Fig. 4, inset.[15]

The proposed mechanism for the stick-slip friction has actually a wide range of applicability. In particular, it describes the transition between elastic and plastic depinning of periodic structures driven through disordered media, such as vortex lattices, charge density waves, and Wigner

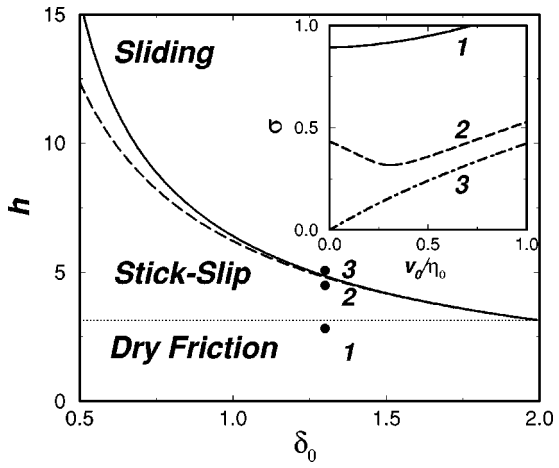

FIG. 4. Temperature- (δ_0) thickness (h) diagram. Above the solid line (h_c) sliding occurs for arbitrary small velocity v_0. Below h_c stick-slips exist for $v_0<v_c$, while the transition to sliding is abrupt with hysteresis between solid and dashed lines and smooth otherwise. Below the dotted line (h_0) one has dry friction without stick-slips. Inset: shear stress σ (or friction force) vs sliding velocity v_0 corresponding to stationary sliding regimes in three different regions. The falling part of line 2 corresponds to the unstable stationary solution; in this range of pulling velocities the system exhibit stick-slip oscillations.

crystals.[13,15] In the case of driven vortex lattices the horizontal axis in Fig. 4, inset, represents voltage and the vertical axes correspond to driving current. Then curve 1 describes the elastic depinning and curve 2 corresponds to hysteretic plastic depinning.

Let us estimate typical values of the critical velocity for the transition to steady sliding. From Fig. 3 one finds a typical value of the velocity $v_c \approx 0.1\eta_*$. In physical units one has $V_c \sim 0.1\eta_0\tau_0 c_s\sigma_0/\mu$. The ratio $\sigma_0/\mu \sim 10^{-2}$ has the meaning of relative stress for onset of plastic deformation in solids. Using the bulk value of $\eta_0 = 10^{10}$ s^{-1} one derives $V_c \approx 1-10$ mm/s, i.e., the value which is about 3 orders of magnitude larger than the experimental value $V_0 \sim 1$ μm/s. Under high pressure η_0 decreases by several orders of magnitude (Refs. 3 and 4 report an effective increase of η_0 by 4–6 orders for pressure of about 20 MPa), and one arrives at $V_0 \sim 0.1$–1 μm/s.

V. NUCLEATION

The above analysis was based on the assumption that the stick-slips occur simultaneously in the entire lubricant layer, which may not be the case for large samples. It is natural to expect that stick-slips occur via a series of nucleation events when droplets of the liquid emerge in the solid phase and then expand and merge throughout the system. Nucleation can be responsible for the observed irregularity stick-slip sequences [notice that the second-order system of ODE's (16) and (17) can only produce periodic oscillations].

If the sample size L is not very large and the ''acoustic shear time'' $\tau_a = L/c_s$ is much smaller than any characteristic time scale of the problem (e.g., slip time), we can simplify the problem by neglecting the dependence of σ on the longitudinal coordinate x, so the shear stress becomes a function of time only.[16] Equation (14) yields

$$\partial_t\sigma + \frac{2\eta_*}{\pi L}\sigma\int_0^L A(x)dx = \frac{v_0}{h}. \tag{21}$$

Here we would like to note that although we derived Eq. (21) from Eq. (14); in fact, Eq. (21) can be derived directly from the stress-strain relation, Eq. (2), even when Eq. (14) is not applicable. In addition, Eq. (21) is much simpler than the original Eq. (14) and, as we will show below, still captures the essential physics of nucleation.

Since during the stick phase A is close to zero, the solid phase can be significantly ''overheated'' by the shear. For $A \ll 1$, integration of Eq. (16) yields

$$A \approx A_0 \exp\left(\int_0^t (-\epsilon+\sigma^2)dt\right), \tag{22}$$

where $\epsilon = 1+\pi^2/h^2-\delta_0 > 0$. From Eq. (21), $\sigma \approx v_0 t/h + \sigma_0$, and A_0 and σ_0 are the values of amplitude and stress in the beginning of stick phase. We restrict ourselves to the case $h \to h_c$, where $\sigma_0 \to 0$ and $A_0 = O(1)$. While σ is small, the amplitude A decays exponentially to very small values. It reaches a minimum $A_{min} = \exp(-2\epsilon^{3/2}h/3v_0)$ at $t_{min} = \epsilon^{1/2}h/v_0$. Then it starts to grow slowly and reaches the value $O(1)$ (slip event) at $t = t_m = \sqrt{3}t_{min}$. At $t_{min} < t < t_m$ the growth rate $-\epsilon+\sigma^2 > 0$, and therefore the lubricant is in an unstable (''overheated'') state. The overheated solid is very sensitive to fluctuations, e.g., to thermal noise. Small nuclei of liquid can appear and expand within the solid, resulting in accelerated slip events. Since nucleation events have probabilistic character, one can expect spatio-temporal randomness of the slip events. However, this randomness can only manifest itself at low noise levels. At the higher level of the noise, the slips become more regular because the number of nucleation sites increases, and the overall effect of the noise averages out. This effect is somewhat similar to the coherence resonance in noise-driven excitable systems where increase of noise makes the oscillations more regular.[17,18]

We studied Eqs. (10) and (21) numerically in a fairly large domain; see Figs. 5 and 6. Since during the slip phase the shear stress rapidly drops, the domains do not necessarily propagate through the entire system and in large systems one may observe ''partial slips.'' The random character of the nucleation process manifests itself in the nonperiodicity of slips and local amplitude A.

In our simulations we used the value $\eta_* = 0.01$, which corresponds to the bulk value of η_0 at normal pressure. For the experimental conditions,[3] the value of η_0 decreases by many orders of magnitude, which makes the simulations technically impossible. However, the qualitative picture of phenomena does not change with a decrease of η_*, which even in our case is already sufficiently small.

VI. SOUND EMISSION

In this section we will briefly discuss the radiation of sound during phase slip events. Although the physical

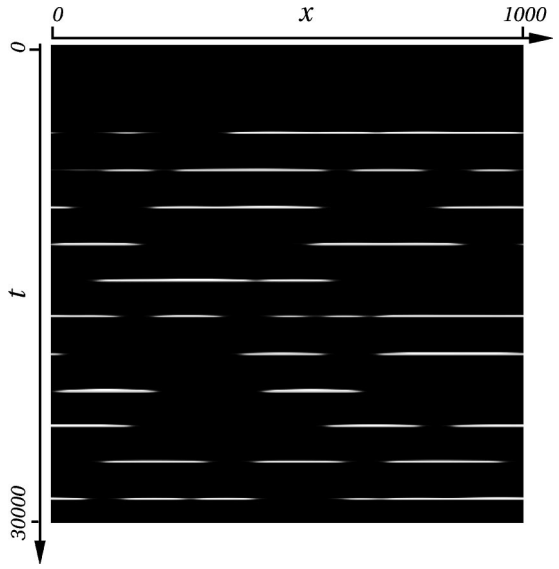

FIG. 5. Space-time plot of A for $\delta_0=1.1$, $h=4, \eta_*=0.01$, and $v_0=0.0002$ in the system of length $L=1000$. Black corresponds to $A=0$ (solid), white to $A=1$ (liquid). Time progresses from top to bottom, total integration time 30 000 dimensionless units. Uncorrelated noise with zero average and amplitude 10^{-16} is added to A at each time step and each grid point.

mechanisms of ultrasound generation in friction experiments are not well understood, it is believed that sound waves in the range from 10^6 to 10^{11} Hz are excited.[2] In most of the mechanisms proposed earlier, the frequency of the ultrasound is proportional to the pulling velocity.

The sound generation can be described within the framework of the full Eqs. (10), (14), and (15) in the regime of ''partial slips.'' Indeed, as follows from Eq. (14), inhomogeneity in $A(x)$ also creates inhomogeneity in the shear stress distribution $\sigma(x)$, which in turns generates elastic waves due to the wave nature of Eqs. (14) and (15).

We studied Eqs. (10), (14), and (15) for the same parameter values as in Sec. V. Indeed, as one sees from Fig. 7 and 8, sound waves are emitted during the slip events. They are manifested as propagating ripples in Fig. 7 and high-frequency modulation in σ vs t profiles.

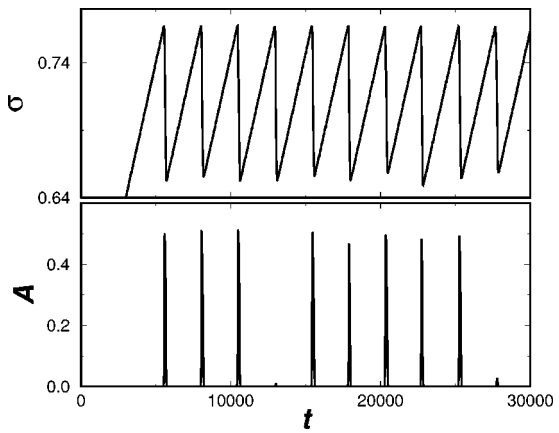

FIG. 6. σ and A at $x=L/2$ vs t for the parameters of Fig. 5.

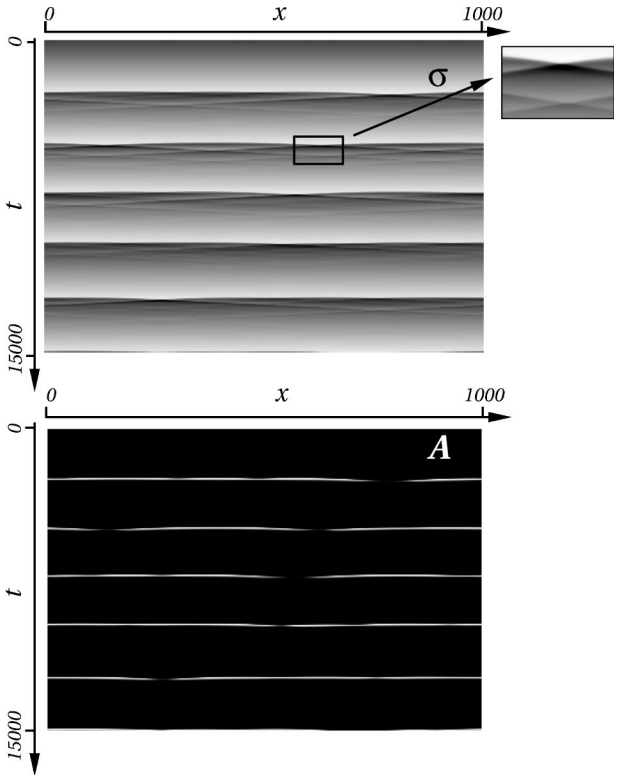

FIG. 7. Space-time plots of σ and A for $\delta_0=1.1$, $h=4, \eta_*=0.01$, $v_0=0.0002$, and $\nu=1$ in the system of length $L=1000$, obtained from solution of Eqs. (10) and (14). Small ripples on the $\sigma(x)$ vs time plot show sound radiation.

It should be noted that sound generation is an interesting phenomenon which can be observed experimentally. According to our results, it is not the reason for stick-slips but their consequence. Our investigation shows that there is no qualitative difference with the nucleation dynamics described in Sec. V, where wave propagation effects are neglected.

Let us now estimate the frequency of the ultrasound. According to our results, the ultrasound is generated during the slip event. Since the duration of slip T_{slip} is of the order

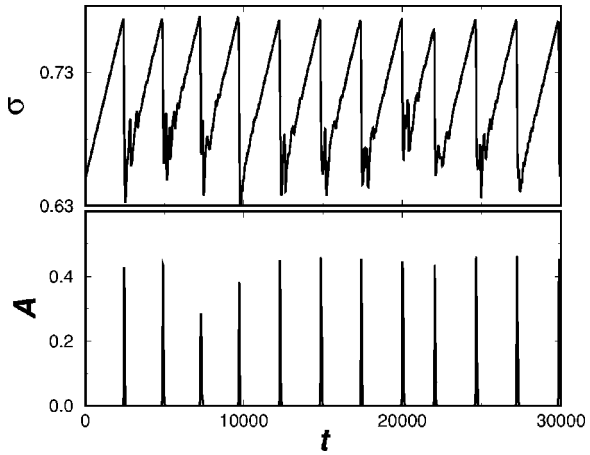

FIG. 8. σ and A at $x=L/2$ vs t obtained from solution of Eqs. (10) and (14), other parameters identical to Fig. 7. Small ripples on the dependence σ vs t are fingerprints of acoustic waves.

$1/\eta_*$, the representative frequency of sound waves will be $\omega \sim \eta_*$. The parameter η changes by several orders of magnitude as a function of applied pressure, and one obtains for the frequency $\omega \sim \eta = 10^6 - 10^7$ Hz for the conditions of experiment.[3] Moreover, our results indicate that the frequency of ultrasound practically does not depend on the pulling velocity. This prediction is worth testing experimentally.

VII. CONCLUSION

In this paper we have proposed a continuous theory for friction dynamics in ultrathin films. Experimentally observed layering and crystallization of ultrathin films near atomically flat surfaces (see, for example, Ref. 3) can be phenomenologically described as an ordered state with the corresponding order parameter close to 1. Under shear stress, crystalline structure breaks, and the film ''melts,'' thereby releasing the stress. This process of shear-induced melting and freezing leads to the stick-slip behavior of thin liquid films to shear-induced melting and freezing processes. Our theory is based on the Ginzburg-Landau equation for the order parameter which describes the melting transition under shear stress. The order parameter then enters the stress relaxation rate so that it approaches zero in the solid state. The developed approach allowed for a quantitative description of dynamic nucleation effects leading to slip events and sound generation. The proposed theory can be applied to a wide range of phenomena including friction in nanoscale devices, friction on ice, etc. A similar approach can be used in describing depinning transitions of flux-line lattices in type-II superconductors, charge density waves, and other structures driven through disorder.[13] Our results may also shed light on various phenomena related to shear thickening and memory effects in complex fluids.[19]

This theory is similar in spirit to our recent analysis of partially fluidized flows in granular materials.[21] That theory also operates with an order parameter equation that is controlled by the shear stress tensor. When applied to the description of granular friction experiments (see, for example, Ref. 20), it also reproduces the observed stick-slip dynamics. The important difference, however, is that the thermodynamic temperature, which is essential here, is irrelevant for the granular dynamics.

It is also interesting to note the analogy between nucleation dynamics of ''partial slips'' in the systems with the lubricated friction and the creation of defects during rapid quench (''cosmological scenario'').[22–24] In the vicinity of the phase transition the defects, e.g., domain walls in the one-dimensional case, are created from small fluctuations of the order parameter on the background of essentially unstable state (overheated solid in our case).

ACKNOWLEDGMENTS

This research was supported by U.S. DOE Grant Nos. W-31-109-ENG-38, DE-FG03-95ER14516, and DE-FG03-96ER14592.

[1] B.N.J. Persson, *Sliding Friction: Physical Principles and Applications* (Springer-Verlag, Berlin, 1998).
[2] E. Meyer, R.M. Overney, K. Dransfeld, and T. Gyalog, *Nanoscience. Friction and Rheology on the Nanometer Scale* (World Scientific, Singapore, 1998).
[3] H. Yoshizava and J. Israelachvili, J. Phys. Chem. **97**, 4128 (1993).
[4] J. van Alsten and S. Granick, Phys. Rev. Lett. **61**, 2570 (1998); H.-W. Hu, G.A. Carson, and S. Granick, *ibid.* **66**, 2758 (1991).
[5] G. Hähner and N. Spencer, Phys. Today **22**(9), 22 (1998); T. Baumberger, P. Berthoud, and C. Caroli, Phys. Rev. B **60**, 3928 (1999).
[6] P.A. Thompson and M.O. Robbins, Phys. Rev. A **41**, 6830 (1990); Science **250**, 792 (1990).
[7] J.P. Gao, W.D. Luedtke, and U. Landman, J. Chem. Phys. **106**, 4309 (1997).
[8] O. Braun, A.R. Bishop, and J. Röder, Phys. Rev. Lett. **82**, 3097 (1999); W. Zhong and D. Tomanek, Europhys. Lett. **15**, 887 (1991).
[9] B.N.J. Persson, Phys. Rev. B **51**, 13 568 (1995).
[10] J.M. Carlson and A.A. Batista, Phys. Rev. E **53**, 4153 (1996).
[11] L. Pietronero, in *Phonons: Theory and Experiments*, edited by P. Brüesch (Springer, Berlin, 1987), Vol. III, Chap. 8.
[12] T.V. Ramakrishnan and M. Yousouff, Phys. Rev. B **19**, 2775 (1979).
[13] A.E. Koshelev and V.M. Vinokur, Phys. Rev. Lett. **73**, 3580 (1994).
[14] R.M. Linden-Bell, J. Phys.: Condens. Matter **7**, 4603 (1995).
[15] V.M. Vinokur and T. Nattermann, Phys. Rev. Lett. **79**, 3471 (1997); M.C. Marchetti, A. Middleton, and T. Prellberg, *ibid.* **85**, 1104 (2000).
[16] The validity of similar conditions of isobaricity in the context of radiative condensation is discussed in detail by B. Meerson, Rev. Mod. Phys. **68**, 215 (1996); I. Aranson, B. Meerson, and P. Sasorov, Phys. Rev. E **52**, 948 (1995).
[17] Y. Braiman, J.F. Linder, and W.L. Ditto, Nature (London) **378**, 465 (1995).
[18] A. Pikovsky and J. Kurths, Phys. Rev. Lett. **78**, 775 (1997).
[19] D.A. Head, A. Ajdari, and M.E. Cates, Europhys. Lett. **57**, 120 (2002); Phys. Rev. E **64**, 061509 (2001).
[20] W. Losert *et al.*, Phys. Rev. E **61**, 4060 (2000).
[21] I.S. Aranson and L.S. Tsimring, Phys. Rev. E, **64**, 020301 (2001); cond-mat/0109358 (unpublished).
[22] T.W.B. Kibble, J. Phys. A **9**, 1387 (1976).
[23] W.H. Zurek, Nature (London) **317**, 505 (1985); N.D. Antunes, L.M.A. Bettencourt, and W.H. Zurek, Phys. Rev. Lett. **82**, 2824 (1999).
[24] I.S. Aranson, N.B. Kopnin, and V.M. Vinokur, Phys. Rev. Lett. **83**, 2600 (1999); Phys. Rev. B **63**, 184501 (2001).